Dispersion Polymerization in Supercritical CO_2 with Siloxane-Based Macromonomer. 2. The Particle Formation Regime

M. L. O'Neill, M. Z. Yates, and K. P. Johnston*

Department of Chemical Engineering, The University of Texas at Austin, Austin, Texas 78712-1062

C. D. Smith and S. P. Wilkinson

Air Products and Chemicals, Inc., Allentown, Pennsylvania 18195-1501

Received September 3, 1997; Revised Manuscript Received February 9, 1998

ABSTRACT: Dispersion polymerization of methyl methacrylate in supercritical CO_2 is studied in situ by turbidimetry at 65 °C from 2000 to 5000 psia for various concentrations of a poly(dimethylsiloxane) monomethacrylate (PDMS−mMA) macromonomer stabilizer. The average particle size, particle number density, and overall surface area are reported vs time during particle formation. Coagulative nucleation and controlled coagulation regions have been identified. They are governed by the amount of stabilizer available relative to the total surface area of the dispersion. Near the end of the controlled coagulation region, which can last tens of minutes, the particle number density approaches the final value. The time in this region is longer than predicted by the model proposed by Paine (*Macromolecules* **1990**, *23*, 3190) due to incomplete incorporation of stabilizer, solubility limitations of polymerized stabilizer in the continuous phase, and plasticization of the particles by CO_2, which increase particle coagulation. Threshold values of pressure and stabilizer concentration are required to achieve a solvent quality and surface coverage sufficient to prevent uncontrolled coagulation during particle formation.

Introduction

Heterogeneous polymerizations in CO_2 have been performed on various monomer systems including methyl methacrylate,[1−4] styrene,[5] 2,6-dimethyl phenol,[6] and acrylamides.[7] Recently PDMS-based macromonomers with a reactive methyl methacrylate group, which form graft copolymer stabilizers in situ during polymerization, have been employed successfully in the dispersion polymerization of methyl methacrylate in supercritical CO_2.[8]

On the basis of experimental results[2,9−11] and modeling of dispersion polymerization,[10] it is assumed that the particle formation regime is complete very soon after polymerization commences, e.g., before 0.1% conversion. After the completion of the formation stage, the particle number density remains essentially constant for the remainder of the polymerization, without the formation of new stable particles.[2,9,10,12] One of the more comprehensive mechanisms of particle formation, the coagulative nucleation mechanism, incorporates the basic phenomenology of homogeneous and aggregative nucleation combined with heterocoagulation of small nuclei and unstable aggregates with larger stabilized particles.[11] This mechanism may be used to describe the effects of stabilizer concentration and solvent strength of the continuous phase. While the effects of these variables have been well studied experimentally in the particle growth regime,[9,11] their roles in the particle formation regime are ill-defined.

Experimental studies have verified the coexistence of unstable nuclei and stable particles during the initial stages of particle formation in dispersion polymerization.[12−14] It has proven difficult to follow the particle formation regime with either electron microscopy[2] or dynamic light scattering(DLS)[12,13] due to the rapid increase in dispersed phase volume fraction and the changing composition of the system. Recently DLS has been used to observe the particle formation stage during dispersion polymerization of MMA and styrene.[12,13] Particle size measurements were limited to the first 3−5 min beyond phase separation, after which multiple scattering began to affect the measurements due to the increase in dispersed phase concentration.

Turbidimetry has been used to study a variety of heterogeneous systems for the determination of particle size,[15−20] stabilization and flocculation of emulsions,[21−23] and particle nucleation in emulsion polymerization.[24] Recent studies of emulsions in supercritical fluids used dynamic light scattering and turbidimetry to quantify emulsion stability, concentration, and particle sizes in situ.[23,25] Compared to other techniques used to measure micron and submicron sized particles,[19,24,26] turbidimetry allows for a higher concentration threshold and can provide very rapid, in situ measurements. For dispersion polymerization, higher conversions may be studied than in the above studies by dynamic light scattering. Turbidimetry may also be performed on systems which are quiescent or turbulent, unlike techniques which measure diffusion coefficients to obtain hydrodynamic radii.

In part 1. of this series,[4] the details of chronology of molecular weight, particle size, product morphology, and stability of dispersions were determined for the particle growth regime in the dispersion polymerization of MMA in supercritical CO_2 with PDMS−mMA macromonomer. The mediocre solvent quality of pure CO_2 for PDMS dictated that monomer need be present in the continuous phase at all pressures studied (1500−4000 psia) to help solvate the PDMS tails and prevent flocculation of the dispersion. Particle size was strongly dependent on stabilizer concentration yet only mildly dependent on pressure above 3000 psi at 65 °C, in agreement with previous studies.[2,8] Finally, it was determined that both a threshold pressure (∼3000 psia) and stabilizer concentration (∼2 wt % stabilizer/monomer) exist below which there is significant change in the polymerization

S0024-9297(97)01315-6 CCC: $15.00
Published on Web 04/17/1998

as indicated by reduced polymerization rates and increased particle coagulation due to insufficient steric stabilization.

The objective of this study is to determine the mechanism of particle formation in the dispersion polymerization of MMA in supercritical CO_2, especially the role of stabilizer, to complement our study of the particle growth regime in part 1. Polymerizations conducted at 65 °C and approximately 20 wt % MMA/CO_2 and 1 wt % AIBN/MMA are monitored at pressures from 2000 to 5000 psia and stabilizer concentrations from 0 to 14 wt % stabilizer/MMA. Turbidimetry measurements as a function of wavelength are used to determine average particle sizes, dispersed phase volume fraction, particle number density, and overall surface area of the dispersion. The pressure is varied to manipulate the solvent quality, which influences the solvation of the PDMS grafts, the solubility of in situ formed graft copolymer stabilizer, and the partitioning of this stabilizer to the interface. The macromonomer concentration is varied to adjust the amount of surface area which may be stabilized. Reaction rates are estimated from dispersed phase volume fractions, and combined with results from part 1 on particle growth,[4] to describe the changing locus of polymerization. Explanations are given for why the results are more complex than those predicted by the model of Paine.[10]

Theory

The turbidity τ is defined in terms of the attenuation of electromagnetic radiation at a scattering angle of 0°

$$\tau = (1/l) \ln(I_o/I) \quad (1)$$

where l is the path length, and I_o and I are the intensities of the incident and transmitted light. In dispersions which scatter but do not absorb the incident light, the turbidity is a function of particle concentration and size and may be calculated from the equation for specific turbidity of Kourti[24]

$$\tau/\phi = 3K^*/2D \quad (2)$$

where D is the droplet diameter, and ϕ is the dispersed phase volume fraction. The scattering coefficient K^* is the ratio of the scattering cross-section to the geometric cross-section. It is a complex function of α, a dimensionless size parameter equal to $\pi D/\lambda$ (where λ is the wavelength of the incident light), and m, the ratio of the refractive index of the dispersed to continuous phase.[15,27] If α and m are known, K^* may be calculated exactly using the Mie theory.[28]

The ratio of turbidities at two different λ is a direct measure of the ratio of scattering coefficients for a monodisperse latex[15,24]

$$\tau_1/\tau_2 = K^*_1/K^*_2 \quad (3)$$

The turbidity ratio method shown in eq 3 is limited to size regimes where the exponential dependence of K^* on λ is high and continuously changing. In this study the measurements are taken in the m range from 1.10 to 1.20 and $1 < \alpha < 10$, where unique solutions for K^* and particle size can be obtained.

For polydisperse latexes, the diameter measured from the turbidity ratio can be related to different moments of the distribution depending upon the values of α and m.[18,24,29] For $1 < \alpha < 10$, the measured diameter is closely related to the weight average particle size ($D_w = (\sum(N_iD_i)^4/\sum(N_iD_i)^3)$. For mildly polydisperse size distributions ($D_w/D_n < 1.1$), the various moments of the distribution are close in magnitude and provide a very close estimate of the weight average so long as particle size and light wavelength are comparable.[16,24]

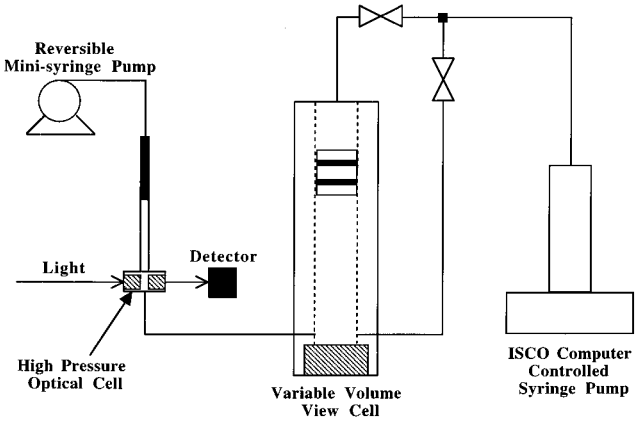

Figure 1. Schematic of high-pressure turbidimetry apparatus.

Once particle sizes have been determined from turbidity ratios, they can be inserted into eq 2 to calculate dispersed phase volume fractions and particle number densities. Errors introduced from experimental uncertainties in the measured particle sizes are magnified in the determination of dispersed phase volume fractions and number densities.

Knowledge of the refractive indices of both phases is required for the determination of particle size. In dispersion polymerization, both dispersed and continuous phases are mixtures of several components. The refractive indices of both phases were estimated using the Lorenz−Lorentz mixing rule[30]

$$(n_{12} - 1)^2/(n_{12} + 2)^2 = \sum \phi_i (n_i - 1)^2/(n_i + 2)^2 \quad (4)$$

where ϕ is the volume fraction of a given component of the mixture and n is the refractive index of the pure component at the same temperature and pressure.

Experimental Section

Materials. Methyl methacrylate (MMA), poly(dimethylsiloxane)−monomethacrylate (PDMS−mMA) with $M_n \sim 10\,000$, and 2,2′-azobis(isobutyronitrile) (AIBN) were obtained from Aldrich and used as received. MMA and PDMS−mMA were purged with nitrogen (Liquid Carbonics, >99.999%) before use. Carbon dioxide obtained from Liquid Carbonics (instrument grade, <20 ppm oxygen) was passed through a Labclear high-pressure oxygen trap (Oxyclear model RGP-R1-300) prior to use. The apparatus was purged with CO_2 prior to reactant introduction.

Apparatus and Procedure. The main components of the new turbidimetry apparatus (Figure 1) were a variable-volume view cell containing a piston,[31] which held the majority of the polymerizing mixture, a computer controlled syringe pump (ISCO model 270D) used to fill the reactor and to control the system pressure, a high-pressure optical cell designed for measuring turbidities, and a motor driven reversible minisyringe pump[32] used to cycle solution between the reactor and the optical cell. Spectra were measured with a Beck-

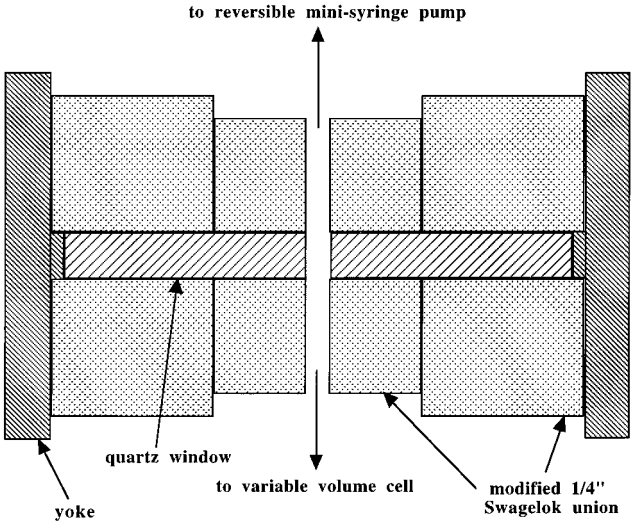

Figure 2. Schematic of high-pressure turbidimetry cell.

man model DU-30 UV−vis single beam spectrophotometer and collected and stored on a PC.

The high-pressure optical cell was constructed out of a $^1/_4$ in. Swagelok union (Figure 2). The interior of the cell was bored out to $^1/_4$ in. i.d., with the exception of a small lip centered in the union which was used as the spacer for the windows. Spacer depths (path lengths) of 0.97 and 0.29 mm were used as measured with a micrometer. On opposite sides, in the middle of the cell, were drilled two holes of ca. 0.2 mm i.d. which entered the cell through the lip. Sections of $^1/_{16}$ in. o.d. stainless steel tubing (0.020 in. i.d.) were welded into the holes. The windows of this cell were made from quartz rod of $^1/_4$ in. diameter and ∼0.7 in. long (aspect ratio of ∼3), and were squared and polished clear with a faceter prior to use. The windows were sealed into the cell with Teflon ferrules, and an aluminum yoke was constructed to hold the windows in place under pressure.

The internal volume of the reversible minisyringe pump was ca. 700 μL, while the volume of the system from the reactor outlet to the inlet of the pump was ca. 200 μL. The cycle rate of the reversible pump was about 15 s, resulting in a flow rate of about 3 mL/min back and forth through the optical cell. The computer controlled syringe pump was set to constant pressure while the minisyringe pump was cycling. As it cycled, the piston inside the reactor would move to maintain a constant pressure. The reactor pressure, monitored with a Sensotech pressure transducer and readout (models TJE−7039−01 and GM respectively), varied less than ±15 psia throughout the reaction.

The magnitude of the pressure drop between the reactor and the minisyringe pump was determined by placing a second pressure transducer and readout at the outlet to the minisyringe pump. At 3000 psia the pressure drop due to flow was a maximum of ±100 psia throughout a cycle of the minisyringe pump.

The reactor was temperature equilibrated with a water bath, while the remainder of the system was kept thermally equilibrated with heating tape and insulation. Three temperature controllers were used to maintain constant temperature throughout the apparatus, while a thermocouple was used to monitor the temperature of the reactor mixture in a tee between the optical cell and the minisyringe pump.

The entire apparatus, with the exception of the variable-volume reactor, was thermally equilibrated to 65 °C prior to introduction of reagents. Known amounts of PDMS−mMA and AIBN were first introduced to the reactor at ambient temperature and pressure. The system was then purged with CO_2 at atmospheric pressure at 100−200 mL/min (gas) for about 10 min prior to the introduction of MMA. The reactor was sealed and charged with a known volume of CO_2.

The reactor was then slowly pressurized to 1500 psia and immersed into a preheated water bath. Stirring of the reactor contents and cycling of the reversible injection pump were commenced as the system was brought to the desired pressure. The contents of the reactor reached 65 °C within 2 min of being placed into the water bath. By 5 min the entire system was thermally equilibrated at 65 °C with temperature fluctuations of less than ±1 °C throughout the apparatus.

Phase separation was noted as the point where the view cell contents began to show an orange tint of color, indicative of Rayleigh scattering by small particles of nucleated polymer. Optical characterization of the polymerizing system consisted of measuring absorbencies from 560 to 660 nm every 2−3 min after phase separation was observed. Each scan took approximately 10 s to complete. The turbidity at 660 nm was also frequently monitored to determine if flocculation or sedimentation occurred during the time required to take a scan. All measurements were taken with the minisyringe pump off and in the fully retracted position to provide reproducible sampling of the reactor contents. Care was taken to try to remove all oxygen from the reactor; however, no attempts were made to remove the inhibitor from the MMA (hydroquinone monomethyl ether, ∼10 ppm). The presence of inhibitor delayed the onset of polymerization and so ensured that thermal equilibrium was reached before polymer phase separation occurred as discussed in part 1.[4] All reactions are compared based on visual phase separation as the start of the polymerization; the reproducibility in determination of the onset of phase separation is estimated to be better than ±1 min.

Results and Discussion

Validation of Turbidimetry for Particle Sizing. The accuracies of turbidity ratios and specific turbidities for calculating particle sizes and dispersed phase volume fraction in our high-pressure cell were determined using a 480 ± 13 nm polystyrene latex standard in water (Polysciences, #07307). The latex concentrations were 0.0210 and 0.105 wt % (± 10%) solids, and the path length was 0.97 mm. Using a refractive index for 1.33 for the water and 1.60 for PS, the measured diameters were 450 ± 60 nm at 0.018 ± 0.003 wt % and 450 ± 50 nm at 0.086 ± 0.010 wt %. Uncertainties in particle size and dispersed phase volume fraction throughout this study were evaluated on the basis of a 0.5% error in turbidity at both wavelengths. Systematic errors in turbidity, such as those introduced by inaccurate path length determinations, manifest themselves in the determination of dispersed phase volume fraction and particle number densities calculated from specific turbidities.

Refractive Indices for the Dispersed and Continuous Phases. In the continuous phase, the refractive index of CO_2 was estimated by extrapolating tabulated data of CO_2 refractive index at 50−65 °C, [33] assuming a temperature independent relationship between refractive index and density (see Table 1). At 65

Table 1. Refractive Indices of Dispersed and Continuous Phases

pressure (psia)	continuous phase (CO_2-rich)		dispersed phase (PMMA-rich)[c]	
	n_{CO_2}[a]	n_{cont}[b]	CO_2 Sorption[d] (wt %)	$n_{particle}$
2000	1.11	1.17	21	1.44
2500	1.15	1.20	24	1.43
3000	1.16	1.21	27	1.43
4000	1.18	1.23	35	1.41
5000	1.19	1.24	42	1.40

[a] Extrapolated from Obriot et al.[33] at equivalent densities to 65 °C. [b] Volume fractions assumed to be that of initial mixture. [c] V_{m,CO_2} (dispersed phase) = 1.0 g/mL;[40] n_{CO_2} (dispersed phase) = 1.2348. [d] Interpolated from Liau and McHugh.[39]

°C the refractive index for pure CO_2 changes from 1.1138 to 1.1969 and the density changes from 0.4955 to 0.8420 g/mL with increasing pressure from 2000 to 5000 psia. A value of 1.4142 was used for the refractive index of MMA.[34] Stabilizer, initiator, and dissolved PMMA were assumed to have a negligible effect on the refractive index of the continuous phase as a result of their relatively minor presence (~1 wt % stabilizer, ~0.2 wt % initiator, and assumed 0 wt % dissolved PMMA).

To our knowledge data are not available on the phase equilibria of ternary mixtures of CO_2/MMA/PMMA. A partition coefficient of 1 on a volume basis is assumed for MMA between CO_2 and PMMA.[35] The phase behavior of an analogous system, CO_2/toluene/silicone rubber, was measured by inverse supercritical fluid chromatography.[36] The partition coefficient changed significantly with CO_2 density below 100 bar but reached a plateau of 2 (concentration in polymer phase to CO_2 phase) for higher pressures of interest in our study. Therefore, a pressure-independent partition coefficient was assumed in this study. The volume fractions required in eq 4 were estimated from weight fractions assuming ideal mixing. Since the maximum conversion to which turbidities could be measured was estimated at ~1%, it was assumed that the refractive indices of both phases were constant throughout the measurements.

The refractive index of PMMA is assumed to be constant at 1.4874,[37] as it has been shown to be invariant for molecular weights larger than 2700.[38] However, the effect of composition on the refractive index of the particle phase is significant due to the high solubility of both CO_2[39] and MMA. To obtain a volume fraction of CO_2 in PMMA, the molar volume of dissolved CO_2 was estimated to be 44 cm^3/mol.[40] The refractive index for CO_2 dissolved in the particle phase is therefore independent of pressure and is estimated to be 1.2348 (the refractive index of pure CO_2 at 65 °C and 44 cm^3/mol).

No corrections were made for the dependence of refractive indices on wavelength as measurements were taken over a small range, i.e., 560−660 nm. Measurement wavelengths were chosen to provide the most accurate data for the particle formation stage. Here there was no absorption of light by any component of the mixture, only light scattering. Table 1 summarizes the values estimated for refractive indices of both phases under various conditions.

To estimate the uncertainty in refractive index and particle size, we assumed that the presence of MMA in the dispersed phase may increase the volume fraction of CO_2 by 25% and that the partition coefficient of MMA may vary from 1.0 to 5.0. It was found that the estimated refractive index of the particle phase shown in Table 1 could vary by ±0.02 with these changes in composition. Since the composition of the continuous phase is more accurately known, it was assumed that the uncertainty in the continuous phase refractive index was ±0.01.

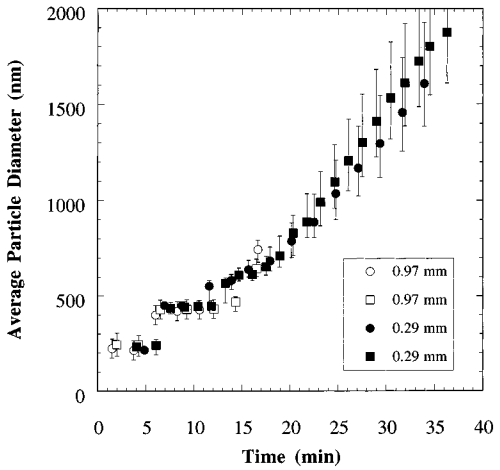

Figure 3. Chronology of average particle sizes determined from turbidity ratios from various path length cells for polymerizations of MMA in CO_2 at 65 °C, 4000 psia with ~5 wt % stabilizer/monomer, and ~20 wt % MMA/CO_2.

Reproducibility and Accuracy of Measurements in CO_2. Multiple scattering effects, which result in deviations from linearity for the turbidity-concentration relationship, eventually become significant as the dispersed phase concentration increases. The result is a concave downward curvature in the turbidity−time profiles and skewing of particle sizes calculated by turbidity ratios toward larger sizes. For the 0.97 mm path length cell multiple scattering begins to affect turbidity measurements after about 20−25 min and after about 35 min for the 0.29 mm path length cell. For this study the turbidity at which multiple scattering prohibits accurate particle sizes from being obtained corresponds to a constant attenuation of incident light for both path lengths for both cells (~5% transmittance at 660 nm). Therefore, smaller path length cells allow for optical characterization of the dispersion to longer times. Data collected after the onset of significant multiple scattering are not used in any calculations.

The chronology of apparent particle size determined from turbidity ratios are plotted in Figure 3. As indicated in our companion study,[4] polydispersity is low throughout the polymerization ($D_w/D_n < 1.1$). Therefore the apparent particle size measured in this study will be closely related to weight average diameter. The agreement between all data clearly exemplifies the ability of the turbidity ratio technique to provide precise and reproducible particle size measurements. Uncertainties in the measured turbidities contribute the majority of the measured errors for particle size at low turbidities, while at higher turbidities uncertainty in the refractive indices of the phases becomes the major contributor. The errors shown in Figure 3 reflect contributions from an uncertainty of ±0.5% in turbidity and the uncertainties in the particle and continuous phase refractive indices listed above. The error bars do not include additional uncertainty from multiple scattering effects at high concentrations.

In Figure 4 the weight average particle size from our companion study by SEM analysis[4] is compared to sizes

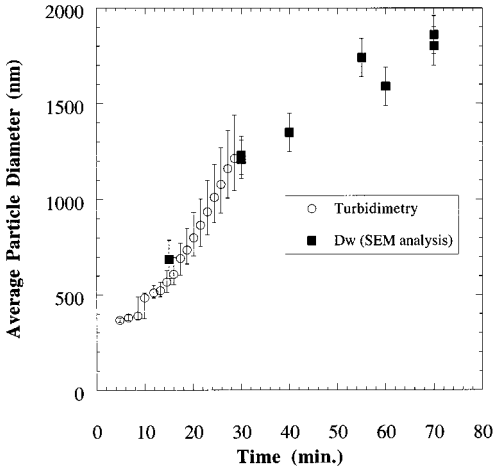

Figure 4. Comparison of chronology of average particle sizes determined from turbidity ratios to weight average particle size from a companion study[4] for polymerizations of MMA in CO_2 at 65 °C, 4000 psia with ~5 wt % stabilizer/monomer, and 25−30 wt % MMA/CO_2.

determined from turbidity ratios for polymerizations at 3000 psia and 25−30 wt % MMA/CO_2. For this figure, the average sizes obtained by turbidity ratios are corrected for sorption of MMA and CO_2 by using the same assumptions for composition outlined above. As a result of the satisfactory agreement between the data over the range of overlap, the above assumptions appear to be reasonable.

Effect of Pressure on Particle Formation. Figure 5a shows the measured turbidities at 660 nm for polymerizations from 2000 to 5000 psia with two different path lengths. The points where multiple scattering becomes significant for both cells are denoted by horizontal dashed lines. Turbidities at 4000 and 5000 psia continue increasing for the duration of measurements; however, those at 3000 psia show a concave curvature toward the time axis at about 50 min. For pressures below 3000 psia, turbidities are low.

Parts b−d of Figure 5 show the chronology of the average particle diameter, particle number density, and total surface area. To determine particle number densities, dispersed phase volume fractions were first calculated from the measured turbidity and average particle size using the eq 2 for the specific turbidity. The particle number density was calculated from the dispersed phase volume fraction and particle diameter. It was normalized to the density of the continuous phase to yield the number of particles per gram of CO_2. Although the PMMA conversion may be determined from the dispersed phase volume fraction, the uncertainty is large due to the unknown partition coefficients of MMA and CO_2 between the phases. The trends in average particle size for these polymerizations are not an artifact of the behavior of scattered light as a function of size.[15,24,27]

For pressures of 3000 psia and higher, two regions may be identified from the data in Figure 5: (1) the coagulative nucleation region, and (2) the controlled coagulation region. The particle number density (Figure 5c) and total surface area (Figure 5d) start very high, indicating the nucleation of a large number of polymer particles from solution. In the first few minutes of the coagulative nucleation region, the number density and surface area decrease sharply as the particle diameter increases rapidly to about 450 nm and then stops at a plateau. At 4000 and 5000 psia, the plateau is brief, lasting only about 5 min. At 3000 psia, it is much longer. The plateaus are reproducible as further indicated by Figure 3. During this plateau, the number density of particles continues to increase(Figure 5c). Studies indicate that separate size populations of very small nucleating material and stable or growing particles may coexist in dispersion polymerizations.[12−14] The periods of constant particle size indicate that the major locus of polymerization is the solution phase and that there is little if any heterocoagulation of unstable nuclei with stabilized particles. The existence of very small nuclei do not affect the measurements of average particle size significantly due to the much greater scattering by the larger stabilized particles. At 600 nm, light scattering by 40 nm particles is ~5 orders of magnitude less than that for 450 nm particles.

After the plateau in particle size, concomitant with the resurgence in average particle size, the particle number density and total surface area decrease. We refer to this period as the controlled coagulation region. Were the flocculation of the latex uncontrolled, a precipitate of undefined size and shape would have been the ultimate product[9] and not a well-defined relatively monodisperse population of particles.[4,8] Controlled coagulation of dispersion polymerizations have been seen previously for systems including PMMA.[9,41] It is assumed that this phenomenology requires a weakly adsorbed stabilizer which can quickly reorganize at the interface to prevent uncontrolled coagulation and a nonviscous dispersed phase which quickly coalesces upon aggregation.[9]

At the start of this controlled coagulation region, which took place after 10 min, a local maximum is observed in the particle density and surface area. Compared with the behavior at higher pressures, the longer plateau at 3000 psia delays the controlled coagulation region. Otherwise, all of the properties in Figure 5 have the same behavior for pressures ≥3000 psia. For example, after 35 min the total surface area for the dispersions is essentially independent of pressure. This result is consistent with the observation that pressure has a relatively minor effect on the final size of the primary particles.[2,4] A minor difference is that the decay in particle density with time is slightly more gradual at 3000 psia than at the higher pressures.

At 3000 psia, the dispersion could be monitored throughout the entire particle formation stage before multiple scattering became significant. At 55 min, the controlled coagulation region ends, producing a constant particle density. The particle number density near the end of the controlled coagulation region is in agreement with the final number density of 10^{10} cm^{-3} at 3000 psia from part 1.[4] Near the end of this region the uncertainty due to multiple scattering grows. This may be the reason the particle density appears to drop below the final value. Conversions at 55 min are estimated to be ~1% based on dispersed phase volume fraction and the above assumptions concerning partition coefficients of MMA and CO_2. Studies of dispersion polymerization of MMA in supercritical CO_2 with PDMS−mMA stabilizer[8] have shown that only a very small fraction (~2.5%) of the total amount of macromonomer becomes incorporated into the particles for stabilization at the end of the polymerization. Since the maximum conversion during our measurements was approximately 1%, the amount of reacted macromonomer available for

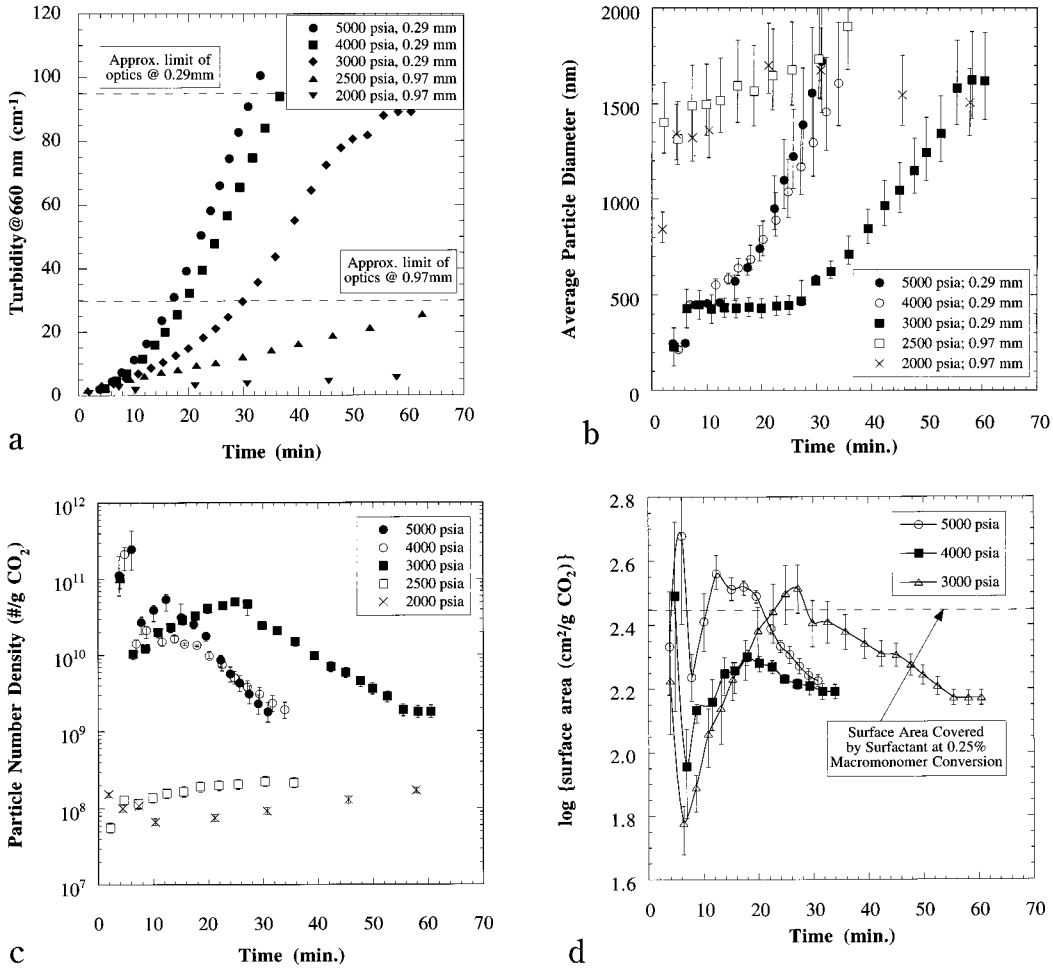

Figure 5. Chronology of (a) turbidity, (b) average particle size, (c) particle number density, and (d) total surface area for polymerizations of MMA in CO_2 at 65 °C, with ~5 wt % stabilizer/monomer and ~20 wt % MMA/CO_2 at various pressures.

stabilization of the particles may be as low as 0.25% of the total macromonomer concentration. The surface area stabilized by the PDMS grafts given by the de Gennes "mushroom" configuration,[42] is $N\pi R_g^2$, where N is the number of macromonomer molecules available for stabilization. If it is assumed that the chain dimensions are the same as for PDMS in a Θ solvent and that 0.25% of the macromonomer is available for stabilization, the calculated surface coverage is given by the dotted line in Figure 5d. In regions where the total surface area is greater than the surface area stabilized, flocculation and coagulation are prevalent as indicated by a decrease in particle density and surface area. After 35 min, the surface area was below the surface area stabilized, and the controlled coagulation, as shown by the average particle diameter, slowed as expected. It is likely that some additional stabilizer may be incorporated during the ensuing growth stage to stabilize the final product.

For lower pressures, i.e., ≤2500 psia, turbidities and particle number densities are low, and much larger particle sizes are measured from the onset of phase separation. At these low pressures the inability of poorly solvated PDMS−mMA based stabilizer to impart stability to the polymerization results in a precipitation polymerization,[4] and particle sizes rapidly become very large. The constant particle size of ~2 μm is likely an artifact of the inefficient sampling of large aggregates and the inability of turbidity ratios to yield accurate particle sizes for very large particles.[15,24,27]

On the basis of the measured dispersed phase volume fractions and the above assumptions concerning MMA and CO_2 partition coefficients (see Table 1), conversion rates during the particle formation stage range from 0.015% min^{-1} at 3000 to 0.033% min^{-1} at 5000 psia. These estimated conversion rates are significantly less than that determined for the particle growth stage (0.83% min^{-1}) from part 1.[4] The differences in rates reflect the changing locus of polymerization from the solution phase during the earliest times to the particle phase for the majority of the polymerization. Higher conversion rates and molecular weights are obtained for polymerization in the polymer-rich phase as the relatively high viscosity suppresses chain termination, i.e., the Trommsdorff effect.

Effect of Stabilizer Concentration on Particle Formation. Parts a−d of Figure 6 show the chronological profiles for polymerizations at 4000 psia with varying amounts of macromonomer stabilizer (0−14 wt %). Increasing stabilizer concentration results in a proportional increase in the total surface area, smaller particle sizes, and higher particle number densities during the particle formation stage. For polymerizations with more than 2 wt % stabilizer, there is little difference in the turbidity profiles; however, the profiles of particle size (Figure 6b) and number density (Figure 6c) vary significantly.

The results for 5.5 wt % stabilizer at 4000 psia were already shown in Figure 5. For 2.2 wt % stabilizer, a very slight plateau is observed in particle size at ~12−

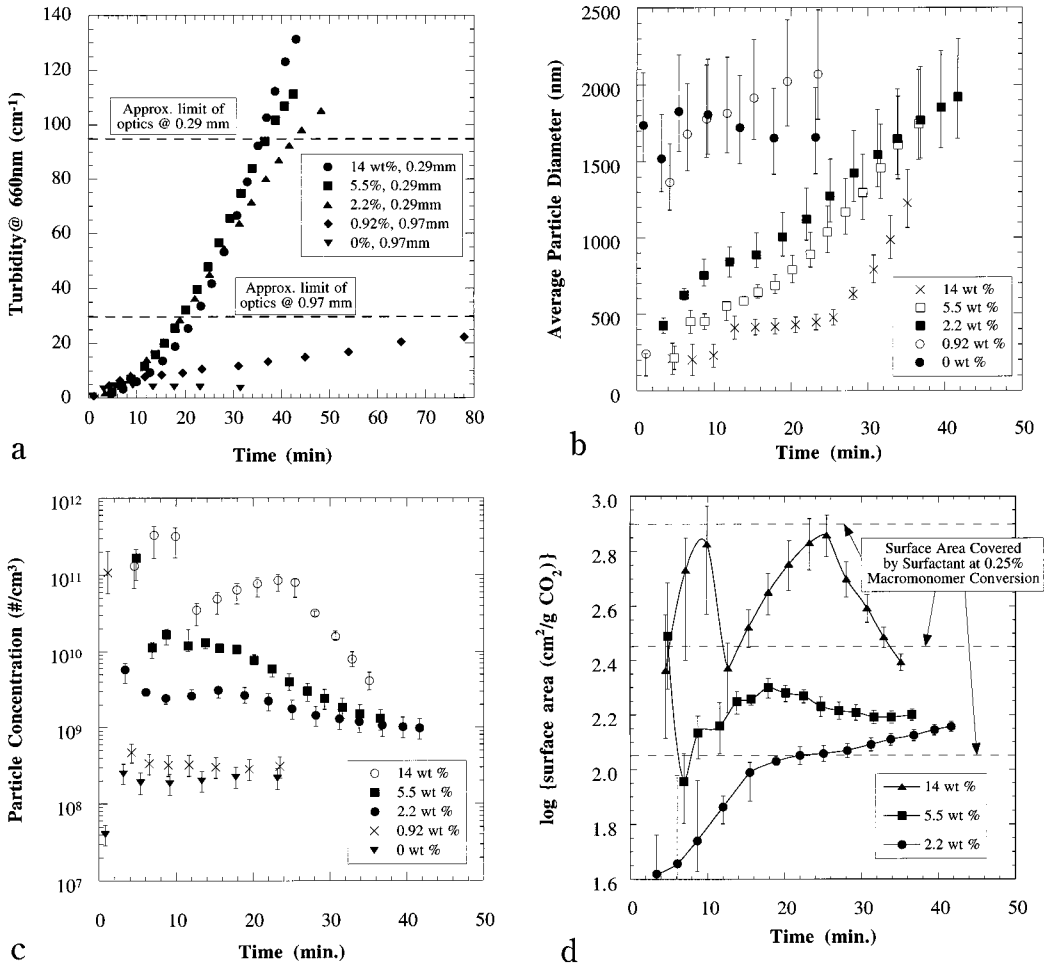

Figure 6. Chronology of (a) turbidity, (b) average particle size, (c) particle number density, and (d) total surface area for polymerizations of MMA in CO_2 at 65 °C and 4000 psia, with ~20 wt % MMA/CO_2 and various stabilizer concentrations.

14 min, for 800−900 nm sized particles. Here, a small local maximum in particle number density is observed at the onset of the controlled coagulation region. Particle number densities are significantly lower relative to polymerizations with 5.5 wt % stabilizer. In Figure 6d the overall surface area generated with 2.2 wt % stabilizer hovers about the estimated surface area stabilized, resulting in continuous nucleation and controlled coagulation of the dispersion, as shown by the very gradual decrease in particle density.

For 14 wt % stabilizer, a plateau begins at 4 min, and a second one begins at 13 min, with a particle size of approximately 450 nm. During each plateau period, particle density and surface area increase rapidly. At the end of each plateau, the surface area went through a maximum and controlled coagulation took place. It was extremely rapid after the first plateau but more gradual in the controlled coagulation region after the second one. The estimated surface area stabilized was the highest for this experiment. Consequently, this experiment also produced the highest particle density, the longest plateau in particle size, and the longest coagulative nucleation region. It is clear from Figure 6d that particle sizes during the plateau regions are governed by the amount of stabilizer available, which appears to be set at an early point (~10 min) into the polymerization.

Polymerizations with <2 wt % stabilizer produce large particles and low particle number densities. As a result of insufficient stabilizer the dispersion coagulates uncontrollably to produce large particles very early in the polymerization, in excellent agreement with part 1[4] and other work.[8,12] Measured sizes and populations are unchanged throughout the measurements, similar in behavior to polymerizations <3000 psia shown in Figure 5. These dispersions also sediment rapidly from the continuous phase.

Table 2. Critical Diameters and Conversions Calculated from Paine's Model

PDMS−mMA concn (wt %) (stabilizer/MMA)	d_{crit} (nm)	X_{crit} (%)
14	64	0.0051
5.5	180	0.024
2.2	450	0.095

Mechanism of Particle Formation and Stabilization. The proposed mechanism of coagulative nucleation and controlled coagulation describes the final particle size and number density successfully. The mechanism is more complex than that described quantitatively in the model of Paine.[10] Paine's model has been applied to polymerization of MMA in CO_2 in part 1 and predicts the final particle diameter successfully.[4] This model describes a single regime of uncontrolled coagulation which ends at a critical diameter, d_{crit}, where the graft available equals the graft required to stabilize the particles. After this point, the particle density is fixed for the remainder of the polymerization. In Table 2, we utilize this model to calculate the critical diameter and conversion for a pressure of 4000 psia.

The calculated critical diameters are somewhat smaller than those observed in our plateau regions and are far smaller than those at the end of the controlled coagulation region. Calculated critical diameters are also smaller than experimental values measured by dynamic light scattering for the dispersion polymerization of MMA with poly(vinylpyrrolidone) as a stabilizer.[12,13] In addition, our observations of a plateau in particle size and a change in the slope of surface area vs time are not predicted by the model.

A variety of factors may contribute to the differences between the model and experimental measurements. The model assumes complete incorporation of the macromonomer onto the surface and assumes that the grafts do not penetrate into the dispersed phase. In our case only a small fraction of the macromonomer is incorporated, and it appears to occur very early, e.g., by the controlled coagulation regime. The increase in particle density in the plateau region may be due to the continued production of stabilizer. Some of the PDMS grafts may penetrate into the dispersed phase since CO_2 is highly soluble in PMMA and acts as a cosolvent for PDMS. The PMMA backbone on the polymerized stabilizer will aid this penetration. Also, the highly plasticized PMMA may be prone to coalescence, as appears to be the case in the controlled coagulation region, especially if the grafts can migrate along the surface. At the end of the controlled coagulation region, the molecular weight is considerably higher. Higher molecular weight will lower CO_2 solubility in the polymer, which will lower the tendency of PDMS penetration into the PMMA. Harder particles with higher PDMS surface concentrations appear to become stable to coagulation.

The controlled coagulation of the dispersion suggests that the stabilizer is easily able to reorganize at the interface and that the dispersed phase is sufficiently fluid to allow the rapid coagulation of the flocculated particles.[9] From this it is inferred that the macromonomer first polymerizes in the solution phase, and stabilization is imparted by adsorption of the newly formed copolymers onto the particle surface, in agreement with the previous studies.[12] Were the macromonomer grafted directly onto the particle surface, reorganization would be expected to be minimal.

Conclusions

Turbidimetry is a very useful technique for studying dispersion polymerization in situ because higher conversions may be monitored than in the case of dynamic light scattering. The entire particle formation stage, which establishes the final particle number density, was monitored by turbidimetry. On the basis of measurement of the particle size, number density, and surface area, coagulative nucleation and controlled coagulation regions have been identified. In the coagulative nucleation region, homogeneous and aggregative nucleation produce an extremely high surface area.[11] These nuclei aggregate and coalesce until the surface area is reduced sufficiently to be covered by the available stabilizer. In minutes, the particle size reaches a plateau, in which the number density and surface area rise to a maximum as coagulative nucleation continues. At the end of the plateau region, the surface area generated exceeds that covered by the stabilizer, and the controlled coagulation region begins. Here, the particle number density and surface area decrease. Near the end of the controlled coagulation region, the measured particle number density was in good agreement with the final particle number density from part 1.[4]

For this system, a pressure of ~3000 psia and a threshold concentration of ~2 wt % stabilizer/monomer are required to prevent uncontrolled flocculation during particle formation. These thresholds are also in good agreement with those determined from part 1.[4] Uncontrolled coagulation occurs when the continuous phase is not a sufficiently good solvent for the stabilizer tail or where there is an insufficient number of stabilizer grafts available during coagulative nucleation.

The Paine model does not predict various experimental observations including a plateau in particle size vs time, the controlled coagulation region for periods up to tens of minutes, and multiple changes in the slope of total surface area vs time. These differences may be caused by incomplete incorporation of stabilizer, solubility limitations of polymerized stabilizer in the continuous phase, and plasticization of the particles by CO_2 which increase particle coagulation and penetration of PDMS into the particles.

Acknowledgment. We acknowledge support from the Separations Research Program at the University of Texas, the National Science Foundation, the Department of Energy, and Air Products and Chemicals. M.L.O. acknowledges support from the Natural Sciences and Engineering Research Council of Canada. In addition, we thank ISCO Corporation for the donation of a high pressure syringe pump. The support of these agencies does not constitute an endorsement of the views expressed in this article.

References and Notes

(1) DeSimone, J. M.; Maury, E. E.; Menceloglu, Y. Z.; McClain, J. B.; Romack, T. J.; Combes, J. R. *Science* **1994**, *265*, 356.
(2) Hsiao, Y.-L.; Maury, E. E.; DeSimone, J. M.; Mawson, S.; Johnston, K. P. *Macromolecules* **1995**, *28*, 8159−8166.
(3) Lepilleur, C.; Beckman, E. J. *Macromolecules* **1997**, *30*, 745−756.
(4) O'Neill, M. L.; Yates, M. Z.; Johnston, K. P.; Smith, C. D.; Wilkinson, S. P. *Macromolecules* **1998**, *31*, 2838.
(5) Canelas, D. A.; Betts, D. E.; DeSimone, J. M. *Macromolecules* **1996**, *29*, 9.
(6) Kapellen, K. K.; Mistele, C. D.; DeSimone, J. M. *Macromolecules* **1996**, *29*, 495−496.
(7) Adamsky, F. A.; Beckman, E. J. *Macromolecules* **1994**, *27*, 312−314.
(8) Shaffer, K. A.; Jones, T. A.; Canelas, D. A.; DeSimone, J. M.; Wilkinson, S. P. *Macromolecules* **1996**, *29*, 2704−2706.
(9) Barrett, K. E. J. *Dispersion Polymerization in Organic Media*; John Wiley and Sons: New York, 1975.
(10) Paine, A. J. *Macromolecules* **1990**, *23*, 3109−3117.
(11) Croucher, M. D.; Winnik, M. A. In *An Introduction to Polymer Colloids*; Candau, F., Ottewill, R. H., Eds.; Kluwer Academic Publishers: Hinghem, MA, 1990; p 35−72.
(12) Shen, S.; Sudol, E. D.; El-Aasser, M. S. *J. Polym. Sci., Part A: Polym. Chem.* **1994**, *32*, 1087−1100.
(13) Lacroix-Desmazes, P.; Guyot, A. *Colloid Polym. Sci.* **1996**, *274*, 1129−1136.
(14) Mandal, T. K.; Mandal, B. M. *Langmuir* **1997**, *13*, 2421−2424.
(15) Melik, D. H.; Fogler, H. S. *J. Colloid Interface Sci.* **1983**, *92*, 161−179.
(16) Wallach, M. L.; Heller, W. *J. Phys. Chem.* **1964**, *68*, 924−930.
(17) Heller, W.; Wallach, M. L. *J. Phys. Chem.* **1963**, *67*, 2577−2583.
(18) Kourti, T. In *Particle Size Distribution: Assesment and Characterization*; Provder, T., Ed.; American Chemical Society: Washington, DC, 1987; p 242−255.
(19) Venkatesan, J. Thesis, Lehigh University, 1993.

(20) Mawson, S.; Yates, M. Z.; O'Neill, M. L.; Johnston, K. P. *Langmuir* **1997**, *13*, 1519−1528.
(21) Vera, M. U.; Durian, D. J. *Phys. Rev. E* **1996**, *53*, 3215−3224.
(22) Reddy, S. R.; Fogler, H. S. *J. Colloid and Interface Sci.* **1981**, *79*, 101−104.
(23) O'Neill, M. L.; Yates, M. Z.; Harrison, K. L.; Johnston, K. P.; Canelas, D. A.; Betts, D. E.; DeSimone, J. M.; Wilkinson, S. P. *Macromolecules* **1997**, *30*, 5050−5059.
(24) Kourti, T. Ph.D. Thesis, McMaster University, 1989.
(25) Yates, M. Z.; O'Neill, M. L.; Johnston, K. P.; Webber, S.; Canelas, D. A.; Betts, D. E.; DeSimone, J. M. *Macromolecules* **1997**, *30*, 5060−5067.
(26) *Particle Size Distribution: Assesment and Characterization*; Provder, T., Ed.; American Chemical Society: Washington, DC, 1987.
(27) Heller, W.; Pangonis, W. J. *J. Chem. Phys.* **1957**, *26*, 498−506.
(28) Bohren, C. F.; Huffman, D. R. *Absorption and Scattering of Light by Small Particles*; Wiley-Interscience: New York, 1983.
(29) Garcia-Rubio, L. H. In *Particle Size Distribution: Assessment and Characterization*; T. Provder, Ed.; ACS Symposium Series 332; American Chemical Society: Washington, DC, 1987, pp 161−178.
(30) Heller, W. *J. Phys. Chem.* **1965**, *69*, 1123−1129.
(31) Lemert, R. M.; Fuller, R. A.; Johnston, K. P. *J. Phys. Chem.* **1990**, *94*, 6021−6028.
(32) McFann, G. J.; Johnston, K. P. *J. Phys. Chem.* **1991**, *95*, 4889−4896.
(33) Obriot, J.; Ge, J.; Bose, T. K.; St-Arnaud, J.-M. *Fluid Phase Equilib.* **1993**, *86*, 315−350.
(34) *CRC Handbook of Chemistry and Physics*, 54th ed.; CRC Press: Cleveland, OH, 1973.
(35) Lu, Y. Y.; Wl-Aasser, M. S.; Vanderhoff, J. W. *J. Polym. Sci., Part B: Polym. Phys.* **1988**, *26*, 1187−1203.
(36) Shim, J. J.; Johnston, K. P. *AIChE J.* **1989**, *35*, 1097−1106.
(37) Brandrup, J.; Immergut, E. H. *Polymer Handbook;* 3rd ed.; John Wiley and Sons: New York, 1989.
(38) Beevers, R. B. *J. Polym. Sci.* **1974**, *12*, 1407−1415.
(39) Liau, I. S.; McHugh, M. A. In *Supercritical Fluid Technology*; Penninger, J. M. L., Radosz, M., McHugh, M. A., Krukonis, V. J., Eds.; Elsevier Science Publishers: Amsterdam, 1985; pp 415−434.
(40) Fleming, G. K.; Koros, W. J. *Macromolecules* **1986**, *19*, 2286−2291.
(41) Fitch, R. M. *Polymer Colloids*, 1st ed.; Plenum Press: New York, 1971.
(42) de Gennes, P. G. *Adv. Colloid Interface Sci.* **1987**, *27*, 189−209.

MA971315A